Iterative image deformation methods in PIV

2002 Meas. Sci. Technol. 13 R1

(http://iopscience.iop.org/0957-0233/13/1/201)

INSTITUTE OF PHYSICS PUBLISHING MEASUREMENT SCIENCE AND TECHNOLOGY
Meas. Sci. Technol. **13** (2002) R1–R19 PII: S0957-0233(02)20239-8

REVIEW ARTICLE

Iterative image deformation methods in PIV

F Scarano

Faculty of Aerospace Engineering, Delft University of Technology, Kluyverweg 1, 2629 HS Delft, The Netherlands

Received 19 December 2000, in final form and accepted for publication 27 September 2001
Published 23 November 2001
Online at stacks.iop.org/MST/13/R1

Abstract
Image processing methods for particle image velocimetry (PIV) are reviewed. The discussion focuses on iterative methods aimed at enhancing the precision and spatial resolution of numerical interrogation schemes.

Emphasis is placed on the efforts made to overcome the limitations of the correlation interrogation method with respect to typical problems such as in-plane loss of pairs, velocity gradient compensation and correlation peak locking. The discussion shows how the correlation signal benefits from simple operations such as the window-offset technique, or the continuous window deformation, which compensates for the in-plane velocity gradient.

The image interrogation process is presented within the discussion of the image matching problem and several algorithms and implementations currently in use are classified depending on the choice made about the particle image pattern matching scheme.

Several methods that differ in their implementations are found to be substantially similar. Iterative image deformation methods that account for the continuous particle image pattern transformation are analysed and the effect of crucial choices such as image interpolation method, displacement prediction correction and correlation peak fit scheme are discussed. The quantitative performance assessment made through synthetic PIV images yields order-of-magnitude improvement on the precision of the particle image displacement at a sub-pixel level when the image deformation is applied. Moreover, the issue of spatial resolution is addressed and the limiting factors of the specific interrogation methods are discussed.

Finally, an attempt for a flow-adaptive spatial resolution method is proposed. The method takes into account the local velocity derivatives in order to perform a local increase of the interrogation spatial density and a refinement of the local interrogation window size. The resulting spatial resolution is selectively enhanced. The method's performance is analysed and compared with some precursor techniques, namely the conventional cross-correlation analysis with and without the effect of a window discrete offset and deformation.

The suitability of the method for the measurement in turbulent flows is illustrated with the application to a turbulent backward facing step flow.

Keywords: image processing, PIV, CIV, window deformation, adaptive resolution, iterative, multigrid

(Some figures in this article are in colour only in the electronic version)

1. Introduction

The particle image velocimetry (PIV) technique has experienced a considerable progress over more than a decade and is still considered as under development. Due to its increased reliability and accuracy the PIV technique has gained the reputation of a powerful and time-effective flow diagnostic method. It is currently employed as a measurement technique for the quantitative whole-field study of complex fluid flows and in several industrial applications.

The growth of the PIV technique due to the improvement of its hardware components is clear: nanosecond pulse duration and high-energy lasers, high-resolution and low-noise interline transfer CCD captors, fast frame grabbers, etc are among the major factors that have raised the quality of the illuminating and recording conditions (Riethmuller 2000).

Nevertheless, digital image analysis methods have an undoubted impact on the performance of the overall measurement technique and often such contribution is more difficult to quantify.

On such a basis a distinction can be made between two specific problems to be solved when performing a PIV measurement. At first, providing the experiment with appropriate flow seeding as well as lighting and an accurate image recording mostly relies on the choice of the hardware configuration. After that, analysing the recordings and extracting most of the embedded information becomes a problem of digital image analysis and depends on a specific algorithm implementation.

The introduction of the PIV technique based on digital technology opened at the beginning of the last decade a remarkable activity in the domain of digital analysis of seeded fluid motion (Utami and Ueno 1984, 1991).

Initial attempts at digital particle imaging (Kimura and Takamori 1986) were viewed with scepticism due to the far lower spatial resolution with respect to the photographic technique, the argument being that the accuracy in the estimate of the displacement was basically given by half the pixel unit (Hesselink 1988). This turned out to be too conservative and estimate of the correlation peak location by means of sub-pixel interpolation was demonstrated to considerably improve the accuracy, with errors as low as one-tenth of a pixel (Willert and Gharib 1991).

However, early approaches to PIV image processing were mostly a reproduction of the optical interrogation technique based on Young's fringe analysis (Cho 1989, Keane and Adrian 1992). The hardware optical correlation was coded with the spatial auto- and cross-correlation functions via numerical Fourier transform of the image intensity field. At the same time it was demonstrated that it was possible to obtain, with relatively low resolution, digital images results comparable to those coming from photographic PIV (Westerweel 1993).

Within less than a decade the literature flourished with investigations focusing on digital algorithms for PIV image analysis resulting in a global effort directed towards the improvement of measurement precision and reliability. A further demonstration of the ongoing development of the PIV technique is the organization of dedicated conferences on a constant basis and the recent worldwide co-operation/challenge project for the assessment of PIV performances (www.pivchallenge.org).

As an indicator of the performance growth it can be mentioned that from the earlier methods to those currently used, the spatial resolution collectively improved with a reduction of the interrogation window size (in pixels). A typical box size of 64×64 pixels or larger, in use at the beginning of the decade, was reduced to a standard of 32×32 pixels, or even to less than 10×10 pixels under prescribed conditions (Hart 1998, 2000, Fincham and Delerce 2000, Lourenço and Krothapalli 1998, Nogueira *et al* 2001).

Moreover, the measurement uncertainty solely associated with the image interrogation procedure was reduced considerably from a typical value of one-tenth of a pixel to a few hundredths or even less (Westerweel 1997, Lecordier 1997, Lourenço 1999, Scarano and Riethmuller 1999 and others). Examples are shown in figure 1.

Despite the recognized maturity of the cross-correlation-based methods, new investigations of the PIV image processing appear in the literature almost on a monthly basis, and often methods with a common mathematical background are given different names or sophisticated acronyms due to a different algorithmic implementation. The result is a misleading picture with an increasing variety of solutions to a common image-processing problem. It is therefore important to attempt to describe some of the common problems encountered in PIV image analysis with traditional tools and, as a counterpart, to discuss some of the different strategies proposed in the literature as advanced methods.

In this paper we discuss correlation-based algorithms under the common denominator of the image matching problem. Finally, an image processing method that proposes an adaptive spatial resolution approach developed by the author is introduced (*window deformation iterative multigrid adaptive resolution*) with details of the performance assessment and with a comparative analysis with predecessor methods.

2. Background

The performance of the PIV technique can be assessed through the evaluation of quality parameters, namely the measurable velocity dynamic range $(u_{\max} - u_{\min})/u_{\min}$ and the spatial resolution Δr. The velocity gradient dynamic range $(\Delta u_{\max} - \Delta u_{\min})/\Delta u_{\min}$ is in most cases a direct result of the above two quantities (Lourenço and Krothapalli 1995). The dynamic range of the velocity gradient is of interest *per se* since it describes important kinematic flow properties (e.g. vorticity, rate-of-strain, divergence) that drive fluid mechanics phenomena. The confidence level R is addressed as the most important parameter when discussing the measurement robustness.

The evaluation of the particle image velocity from a digital pair of recordings is usually composed of two separate problems. The *image processing* returns the displacement (i.e. velocity) vector distribution from the particle image of the recordings. The *data validation* detects the presence of spurious measurements on the basis of selected criteria such as correlation signal-to-noise ratio S/N (Keane and Adrian 1992), local median thresholding (Westerweel 1994), correlation map symmetry (Rohaly *et al* 2000) among others. Often these two steps are kept separate and the data validation is performed only at the end of the evaluation. However, it should be mentioned that with recursive methods that repeat

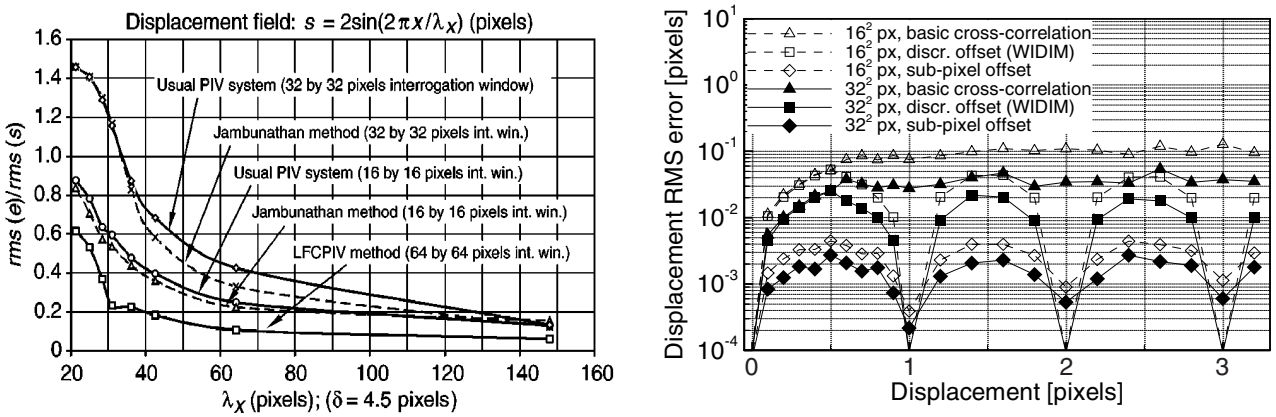

Figure 1. Left: performance comparison of the cross-correlation method, the local field correction (LFC) method (Nogueira *et al* 1999) and an iterative image distortion method (Jambunathan *et al* 1995). Right: performance of cross-correlation methods: ▲ basic cross-correlation; ■ discrete window offset; ♦ iterative multigrid window deformation (Scarano and Riethmuller 2000).

the image evaluation several times, image processing and data validation might mutually interact.

The following part of the discussion focuses on the image-processing problem that aims at improving and assessing the velocity measurement precision. Only the case of single-exposure image analysis is discussed since nowadays this recording mode is properly supported by standard hardware in the majority of cases.

It is common for researchers investigating new methods to compare their performance with a benchmark method. In the case of PIV image processing the reference method is the numerical cross-correlation function. Its most important features are:

- a rectangular region (interrogation window) is selected at a prescribed location on each recording;
- the cross-correlation is performed over the two windows;
- the location of maximum correlation is identified;
- the sub-pixel estimate of the above location is obtained via local interpolation.

Willert and Gharib (1991) proposed the use of a three-point Gaussian fit for the peak interpolation and this choice is still widely adopted.

The normalized cross-correlation function reads as

$$\phi_{fg}(m,n) = \frac{\sum_{i,j=1}^{M} f(i,j)\, g(i-m, j-n)}{\sqrt{\mathrm{cov}(f)\mathrm{cov}(g)}} \qquad (2.1)$$

where f and g denote the grey intensity distribution over the interrogation areas (with mean value subtraction). The denominator is the product of the image covariance over the respective interrogation windows.

The parameters that most influence the measurement error ascribed to the recording process are the particle image diameter, the particle image density, the particle image contrast, the out-of-plane displacement and the in-plane image deformation associated with the velocity gradient.

Several authors have investigated the influence of these parameters on the measurement uncertainty (Keane and Adrian (1990), Westerweel (1993), Boillot and Prasad (1996), Raffel *et al* (1998) among others). Although discussion is still open on the subject there is general agreement concerning some points:

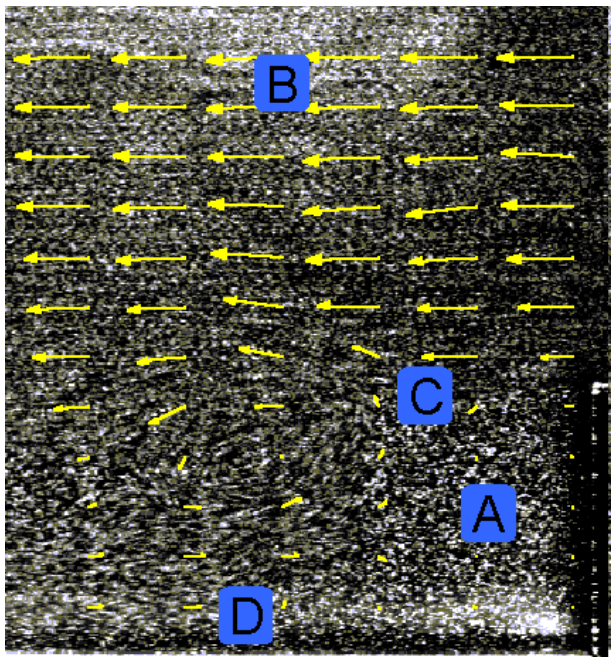

Figure 2. Instantaneous tracer pattern (the two exposures are added in order to visualize the particle displacement) and velocity distribution. The labelled squares indicate the interrogation window size (64 × 64 pixels).

- The velocity dynamic range is limited due to the conflict between the interrogation window size and the in-plane displacement that causes 'loss of pairs' (Adrian 1991).
- A velocity bias (systematic underestimation) occurs, due to the finite extent of the interrogation window, resulting into a trade-off between accuracy and spatial resolution (Westerweel 1993).
- The fractional displacement estimate is dependent on the peak interpolation function. A typical form of error introduces a bias towards integer values of the displacement bringing the measurement accuracy back to its 'discrete nature'. The phenomenon is thus referred to as 'peak locking' (Westerweel 1993, Lourenço 1996).
- Peak locking error also occurs when the particles images

are sampled at a poor spatial resolution (particle image size smaller than two pixels).
- The correlation peak signal drops in regions with a large velocity gradient. Loss of pairs is due to the particle image pattern deformation.
- The spatial resolution of the method is limited by the minimum number of particles in the interrogation window.

These points are discussed below, qualitatively observing the behaviour of the correlation signal when critical conditions are met with respect to the mentioned problems.

Figure 2 shows an example of a typical PIV experiment in a turbulent shear flow. The seeding density is relatively uniform and some spurious reflections occur close to the solid walls. Some conclusions can be drawn about the characteristics of the correlation signal in different regions of the flow. In region A the fluid is practically at rest and the correlation map is expected to show a maximum located close to the origin and well distinguished from the noise (figure 3, left).

At location B a significant loss of particle pairs occurs due to the in-plane displacement. In fact, since the displacement is of about ten pixels and the window size is 64×64 pixels, the resulting matching area is reduced of about one-sixth. The resulting correlation signal is weaker (figure 3, right).

When dealing with the highly sheared flow at C, the deformation of the particle image pattern between the two exposures becomes critical: the correlation peak becomes broader and multiple peaks can occur in the direction where the velocity exhibits the larger variation along the interrogation window (figure 4, left). This behaviour is undesirable since it leads to a higher measurement noise for those regions where interest is often focused, such as boundary layers, shear layers or vortices.

Finally, when approaching an optical interface (most commonly a solid boundary as in region D) spurious reflections mask the particle image pattern. The resulting correlation map is affected by a noise pattern aligned in the same direction as the interface (figure 4, right).

The remainder of this paper focuses on the third case from the above example, namely the problem of correlating a particle image pattern that is deformed by a large velocity gradient. Some concepts of kinematics and visual motion are first introduced, in order to then discuss different approaches to the problem proposed in the literature.

3. Cross-correlation image matching

Consider the planar motion of a fluid element containing a tracer pattern (figure 5). The spatio-temporal evolution of the tracers within the fluid element constitutes a succession of mappings that produce each image from the previous one. For each neighbourhood at time t_1 the mapping can be expressed in terms of the local displacement $\boldsymbol{d}(x, y)$ of the neighbourhood at a location $\boldsymbol{r}$ that produces the corresponding neighbourhood in the next image at time t_2 in the sequence.

The image flow velocity can be defined as the time rate of change $u(x, y, t)$ (Horn and Schunk 1981) of the mapping displacement field $d(x, y, t)$.

As was anticipated, most PIV interrogation techniques rely on the cross-correlation function to determine the (image) flow velocity from particle image pairs.

With a degree of generality, the application of this operator can be interpreted as an optimization process:

$$\max_{d} \int_W f\,(x, y)\, g\,(x + \Delta x, y + \Delta y)\ \mathrm{d}x\,\mathrm{d}y \tag{3.1}$$

where $d = (\Delta x, \Delta y)$ is the vector parameter to be determined that maximizes the correlation function between the functions $g(x, y)$ and $f(x, y)$. The formula yields under certain hypotheses the most probable tracer displacement over the ensemble of tracers that belong to the interrogation region W (Adrian 1991).

For an image pair the velocity within the interrogation region is then approximated by the expression

$$u \approx \frac{d}{t_1 - t_2}. \tag{3.2}$$

It is clear that equation (3.1) yields an exact match (unit correlation peak intensity) when the displacement is uniform across the interrogation window.

A higher degree of generality is obtained when the optimization is performed considering the displacement spatial distribution

$$\max_{\Delta x, \Delta y} \int_W f\,(x, y)\, g[x + \Delta x\,(x, y)\,, y + \Delta y\,(x, y)]\,\mathrm{d}x\,\mathrm{d}y. \tag{3.3}$$

In this case the intensity distribution in the function $g(x, y)$ is evaluated considering a displacement distribution that varies spatially over the interrogation window.

The implementation of such a method implies that the two windows are subjected to a relative translation matching (performed by ordinary cross-correlation) and to the relative deformation.

The output of such an operator depends on the spatial distribution of the displacement over the interrogation window. When the imposed spatial distribution of the displacement corresponds to the actual displacement field, the two images are expected to produce the maximum match.

The displacement distribution over the finite interrogation region is estimated by means of a Taylor series:

$$\begin{aligned} u\,(x, y) = {} & u\,(x_0, y_0) + \left(\frac{\partial u}{\partial x}\right)(x - x_0) \\ & + \left(\frac{\partial u}{\partial y}\right)(y - y_0) + \cdots + \frac{1}{2!}\left[\left(\frac{\partial^2 u}{\partial x^2}\right)(x - x_0)^2\right. \\ & + \left(\frac{\partial^2 u}{\partial x \partial y}\right)(x - x_0)\,(y - y_0) \\ & \left. + \left(\frac{\partial^2 u}{\partial y^2}\right)(y - y_0)^2\right] + \cdots + \mathrm{o}\,(x - x_0)^3 \end{aligned} \tag{3.4}$$

with

$$x \in \left[x_0 - \tfrac{1}{2}W, x_0 + \tfrac{1}{2}W\right] \quad \text{and} \quad y \in \left[y_0 - \tfrac{1}{2}W, y_0 + \tfrac{1}{2}W\right].$$

In the above expression $(x_0,\ y_0)$ denotes the centre of the interrogation window W.

When the optimization described in equation (3.4) is implemented using the Taylor series to describe the displacement, the number of parameters that play a role in the optimization depend directly on the order of the truncated Taylor expansion. The number of parameters used in the optimization process increases with increasing order of the series expansion as discussed by Tokumaru and Dimotakis (1995).

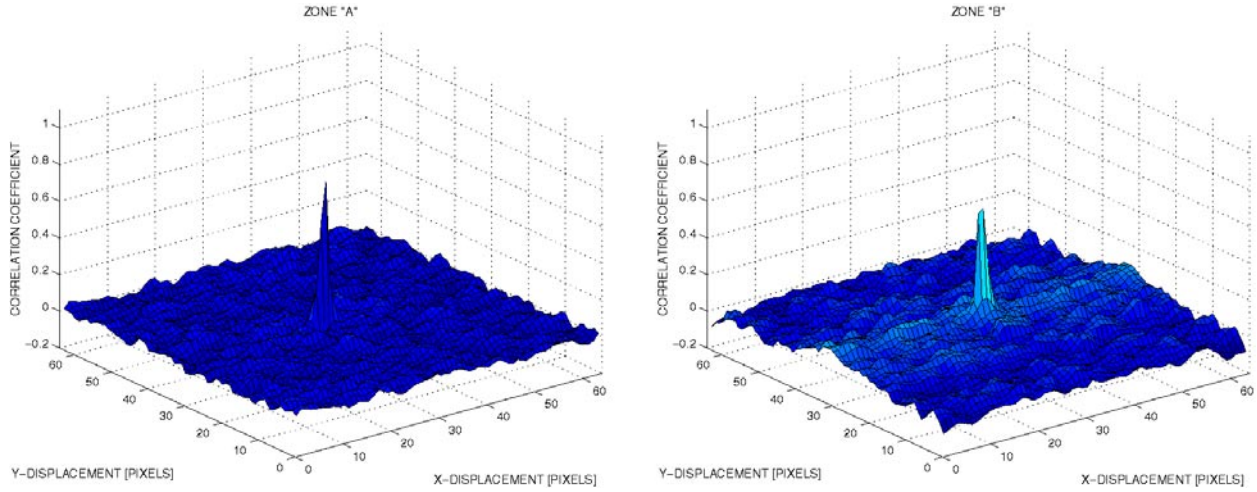

Figure 3. Correlation map corresponding to region A (left) and B (right).

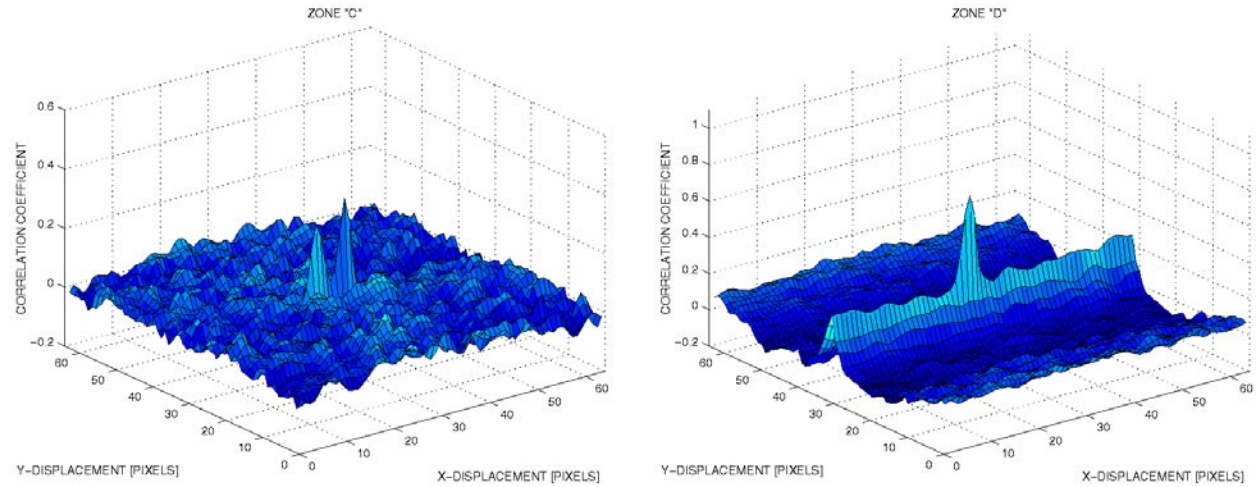

Figure 4. Correlation map corrresponding to region C (left, note the smaller vertical scale) and D (right).

Table 1 summarizes the situation for the two-dimensional problem. The computational effort for the direct correlation is used as a reference and is given by N^4 where N is the linear size in pixel of the correlation window. It should be added that the computational cost for the case of $p \geqslant 1$ is further increased by the necessary operation of image interpolation at sub-pixel locations, which is discussed later. Considering the overall computational effort, it is clear that the method can be implemented only when the Taylor series is truncated at a low order.

Several methods currently adopted follow a different approach to the problem of higher-order image matching. If an estimate of the displacement field is available, for instance by conventional cross-correlation analysis, then such a result can be used to apply the convection equation to the scalar intensity field. Then the subsequent interrogation is still performed via cross-correlation, but the argument functions (the particle image windows) are selected in such a way that the image matching is augmented.

The two-dimensional cross-correlation can be rewritten as

$$\phi_{fg}(m,n) = \left\{ \sum_{i,j=1}^{M} f\left(i + \frac{u_p \Delta t}{2}, j + \frac{v_p \Delta t}{2}\right) \times g\left(i - m - \frac{u_p \Delta t}{2}, j - n - \frac{v_p \Delta t}{2}\right) \right\} \times \left\{ \sqrt{\mathrm{cov}(f)\mathrm{cov}(g)} \right\}^{-1} \tag{3.5}$$

where u_p and v_p represent the components of the spatial (image) velocity distribution as obtained by means of the previous image interrogation.

It should be remarked that when the inserted u_p and v_p are the actual velocity components distribution, then a peak will appear exactly at the origin of the correlation map of approximately unit value.

3.1. Building the predictor displacement field

In the previous discussion the Taylor series expansion is hypothesized to locally describe the displacement function using a limited number of parameters. Figure 6 depicts the effect of the first three terms of the Taylor expansion

Table 1. Parameters participating in the optimization procedure with increasing order of the series expansion.

Truncation order	0	1	2
# Parameters (p)	2	6	12
Yield	u, v	$u, v, u_x, u_y,$ v_x, v_y	u, v, u_x, u_y, v_x, v_y $u_{xx}, u_{xy}, u_{yy}, v_{xx}, v_{xy}, v_{yy}$
# Computations	$(N^2)^2$	$(N^2)^6$	$(N^2)^{12}$

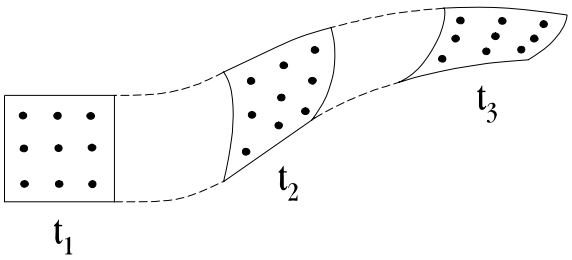

Figure 5. Motion of a fluid element and tracers.

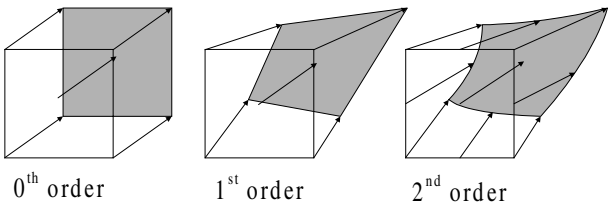

Figure 6. The effect of window deformation with a different truncation order of the displacement distribution.

on the displacement predictor, and therefore on the relative transformation of the correlating window.

Several methods are listed in the literature that make use of such a displacement prediction. It is possible to establish a classification depending on the order of the polynomial in the Taylor expansion.

It should be clear that the ordinary cross-correlation method reduces to the case of $d(r) = 0$ everywhere, therefore no predictor displacement is applied *a priori* when the correlation is computed.

3.1.1. Zero-order displacement predictor. Two of the most popular interrogation methods fall into this category:

(a) One-step direct correlation with different size of the interrogation window and search area. The algorithm is described and performances are analysed in detail in several studies (Adrian 1998, 1991, Keane and Adrian 1990, Fincham and Spedding 1997, Westerweel 1997, 2000, Gui *et al* 2000, 2001). In this case the translation displacement is accounted for by the increased extent of the search area (figure 7) and the problem of loss of pairs due to in-plane motion is partially solved. Among the advantages of the method are the simple implementation and reliability as well as the low computational cost.

(b) Multi-step cross-correlation with a discrete window offset (Westerweel et al 1997). The displacement prediction is obtained by a conventional cross-correlation analysis and the result is applied uniformly to shift the interrogation windows

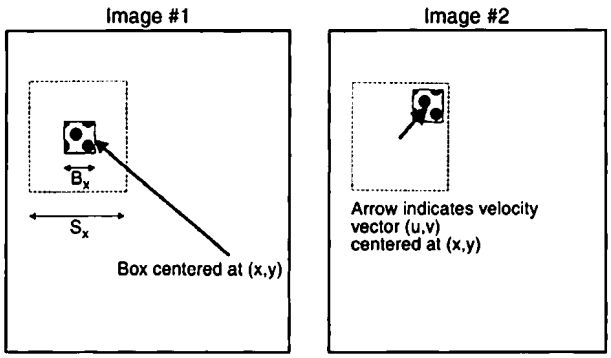

Figure 7. Correlation window and search area (from Fincham and Spedding (1997)).

one with respect to the other. The method significantly improves the performances of ordinary cross-correlation with a higher S/N and a higher measurement precision. An additional advantage of the method is its suitability for the multigrid implementation (Scarano and Riethmuller 1999) that allows one to improve the spatial resolution.

It is important to remark that applying a symmetric window shift with respect to the interrogation location results in a central difference interrogation (CDI) (Wereley and Meinhart 2000); see figure 8. Compared with the usual forward shift interrogation (FDI), such a scheme has the advantage of being second-order time accurate, and therefore yields a considerable improvement when a large time delay occurs between exposures.

Therefore, the result of the correlation of the two windows should be located on the mean position between the centre of the interrogation window and that of the search window. This method also has a relatively low computational cost which is comparable to that of ordinary correlation (multiplied by the number of iterations).

In terms of image deformation, the above two methods apply piecewise uniform displacement prediction to the whole particle image recordings.

(c) Multi-step iterative sub-pixel window offset. This method is a variation of the previously mentioned ones in that the value of the displacement predictor is not limited to integer numbers. As a dramatic consequence, when displacing the interrogation windows, the image intensity is required at intermediate locations between pixels. Therefore, an image interpolation procedure must be applied in order to retrieve the light intensity at those locations pointed to by the displacement predictor. The method claims a considerable improvement in precision and accuracy with an error level of the order of 10^{-2} pixels, as assessed with synthetic images (Lecordier 1997). The image interpolation scheme becomes a

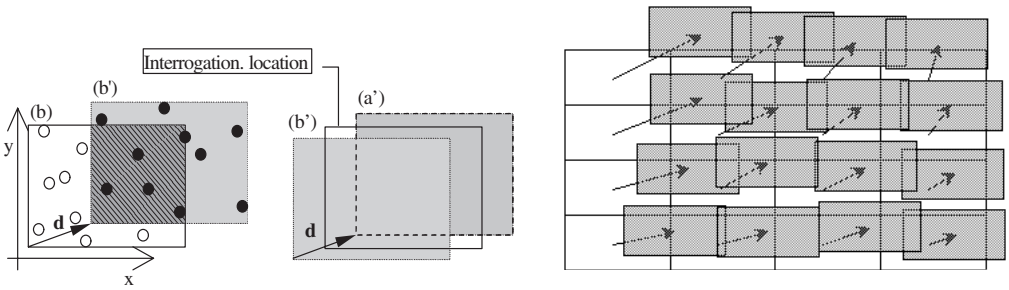

Figure 8. Window shift method with FDI (left) and with CDI (right). Piecewise uniform displacement predictor distribution.

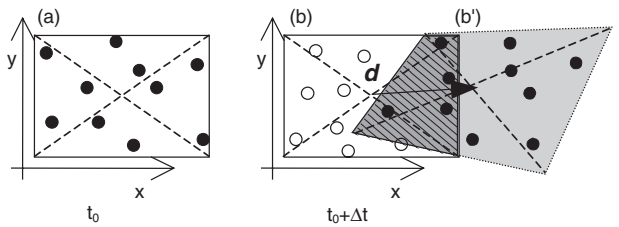

Figure 9. Schematic illustration of the image transformation due to linear in-plane motion. Particles follow the mean displacement $\boldsymbol{d}$ (translation) and the local displacement gradient.

crucial aspect in such a procedure and it must be consistent with signal theory. Suitable schemes must be adopted so as to avoid or minimize image degradation or signal loss (Niblack 1986). Common choices are multidimensional polinomial interpolation (bilinear biquadratic, bicubic splines) and regression formulae such as least-squares biquadratic.

3.1.2. Linear displacement predictor. When the displacement distribution is obtained after a first image interrogation, the continuous displacement distribution (piecewise linear) can be estimated using a two-dimensional linear interpolation with respect to the interrogation grid points (figure 9).

Huang *et al* (1993b) contributed to the development of such an approach, proposing the particle pattern image distortion (PID) technique. The major goal of the technique was that of maximizing the effective particle image pattern (PIP) matching during the cross-correlation analysis. As a result, the technique brought a significant improvement, enlarging the vorticity dynamic range with respect to conventional cross-correlation. The work is widely referred to in subsequent literature studies that followed similar approaches. The authors showed that the distortion of the interrogation window allowed the measurement of the particle image displacement over a larger range of the velocity gradient with respect to the traditional correlation. The maximum velocity gradient measured was 55.3 s^{-1} (1.1 pixel/pixel deformation rate) compared with 15 s^{-1} (0.5 pixel/pixel) from Willert and Gharib (1991). However, the analysis of synthetic images of a simulated Oseen vortex yielded a measurement uncertainty of about 0.25 pixels, which is relatively high, presumably due to the low-accuracy centroid scheme used for the determination of the correlation peak sub-pixel location.

The results obtained on a water flow past a backward-facing step ($Re_h = 4000$) with a comparison of PIV and the PIP method are reported in figure 10. Clearly it is possible to enlarge the range of the measurable velocity gradient. The effectiveness of the image distortion procedure is proven by the higher S/N level (consequently a lower yield of spurious vectors) in the highly sheared/vortical region downstream of the separation point. In comparison, the conventional cross-correlation for a given choice of the S/N threshold fails in the region of higher vorticity.

However, the method was implemented with a high computational cost since there was a high resolution associated with the dense data spacing obtained by means of a large overlap between adjacent windows.

Moreover, a relatively simple image reconstruction scheme (bilinear interpolation) and the sub-pixel correlation peak fit (centroid) are considered inaccurate for the image resampling and for the correlation peak location estimate, as was demonstrated in later studies (Westerweel 1993, Lourenço 1996). Therefore, the above implementation did not completely succeed in exploiting the benefit of the image deformation philosophy in terms of measurement precision.

A method similar to PID was proposed by Jambunathan *et al* (1995) who also evaluated the method's performance by means of synthetic PIV images with a known particle image displacement.

The choice of the displacement distribution to test the method performance was made on the basis of physical considerations; namely, the Helmoltz velocity theory was invoked that divides the movement of a fluid element into three subsidiary terms:

$$V(r) = V_0 + \tfrac{1}{2}\Delta V \delta r + \nabla\phi \tag{3.6}$$

where $V(r)$ is the velocity distribution across the fluid element. The three terms in the right-hand side of the equation are translation, rotation and bi-axial shear, respectively.

The two most important outcomes were that (a) the measurement accuracy can be improved from a factor of 2 to 5 using the image deformation method and (b) the correlation peak height is weakly dependent of the in-plane displacement distribution.

The assessment of the method returned a measurement error level of only 0.02 pixels on synthetic particle images with a uniform displacement. Although much emphasis was given to the pattern matching algorithm, the image re-sampling process was performed with a bilinear interpolation, which has a relatively low accuracy compared with higher-order interpolation schemes.

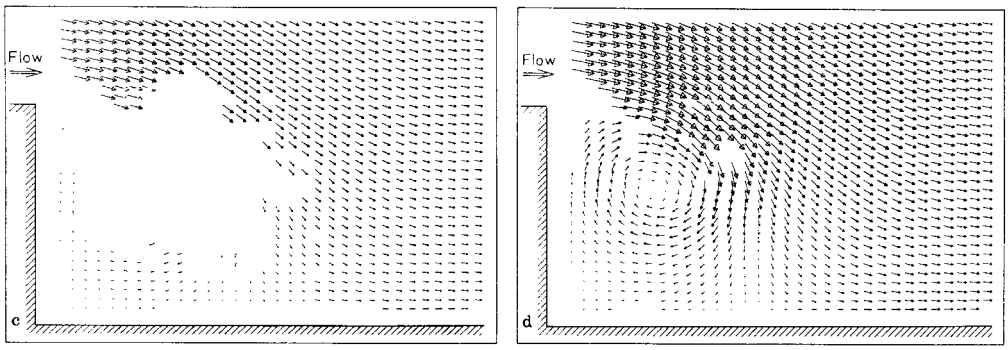

Figure 10. Comparison between results as obtained with the conventional (left) and the PID technique (right) for the measurement of the water flow downstream of a backward-facing step (Huang *et al* 1993).

A method referred to as window (displacement) deformation iterative multigrid (WIDIM) has been proposed by the author on the trend-line of the PID method. Several points of improvement were exploited concerning the accuracy of the correlation sub-pixel interpolation (three-point Gaussian fit) and the image interpolation scheme (two-dimensional cardinal interpolation formula with Whittaker reconstruction (Pratt 1978)). Moreover, the method demonstrated that the image distortion technique could be successfully combined with multigrid interrogation with the progressive window refinement method. The method's performance was assessed by means of synthetic PIV images. The results showed that an error level below 10^{-2} pixels could be obtained. A detailed description of the results is provided in the remainder of this paper.

3.2. Higher-order methods

Tokumaru and Dimotakis (1995) investigated an image analysis technique referred to as correlation image velocimetry (CIV). The authors adopted a method that utilizes the concepts of domain transformation defined on the basis of the image flow mapping with correlation. The global optimization process that relies on the minimization (in a least-square sense) of a Lagrangian operator properly defined was implemented. The expression of the optimization process reads as

$$\min_{\xi(x,t_0),\,\xi(x,t_1)} \int_V \left(\{c_1[\xi\,(x,t_1)] - c_0[\xi\,(x,t_0)]\}^2 + \sigma^2 \right) \mathrm{d}^2x. \tag{3.7}$$

An appropriate choice of the smoothing function, σ^2 is needed.

Here $\xi(x,t_0)$ and $\xi(x,t_1)$ represent the Lagrangian displacement field at two subsequent time instants while $c(\xi)$ is the *transported* scalar field. The present method restricts the form of the displacement field to a truncated (Taylor) series approximation (equation (3.4)). As previously remarked, the higher the order of the approximating series the larger is the number of parameters to be considered in the optimization, and therefore the computational cost increases exponentially with the series order.

The validity of such a method was assessed in the application to laboratory flows (Couette flow between concentric cylinders, cylinder-wake flow (figure 11)) as well as atmospheric flows (Voyager images of Jupiter).

Such an interrogation method is conceived to perform a global optimization of the correlation coefficient in a multidimensional space where not only the displacement component are considered as optimization parameters but also the local spatial derivatives of the displacement.

The CIV technique lists several advantages with respect to a basic correlation method: (a) a multi-dimensional correlation function locally estimates the velocity and the deformation rate, (b) the method is suitable for the analysis of a generic tracer motion and the tracer pattern does not need to be of particle type as is common in PIV and (c) a higher spatial resolution can be achieved since the velocity derivatives and the associated relevant flow quantities (vorticity, strain-rate, divergence) are measured at each independent interrogation spot. In comparison, ordinary cross-correlation analysis requires the velocity derivatives to be estimated by finite differences of the velocity data evaluated at neighbouring grid locations. However, a detailed assessment of the CIV method has not been performed.

A recent study (Ruan *et al* 2001) proposes to perform the optimization process previously described at a lower computational cost by means of local rather than global optimization. The method is referred to as direct measurement of vorticity (DMV) and performs the direct evaluation of the vorticity from the analysis of the image flow rotation. The vorticity is associated to the PIP rotation, therefore after the polar coordinates transform, the cross-correlation of the transformed PIP yields directly the local rate of rotation. Figure 12 shows the PIP in the physical x–y plane and its mapped counterpart MPIP after the transformation in polar coordinates r–φ. A rotation in the x–y plane corresponds to a simple translation in polar coordinates, which can be evaluated applying the cross-correlation operator.

The main advantages of the method are a higher spatial resolution and the de-coupling of the measurement error of velocity and vorticity. In fact, small errors on the velocity do not directly affect the evaluation of the vorticity.

The performance assessment on synthetic images of an Oseen-vortex displacement distribution yielded promising results with a noise level of the DMV method comparable to that coming from conventional PIV results and finite differences.

Fincham and Delerce (1999) proposed an advanced CIV technique. The method called *peak anti-aliasing spline transformed interrogation scheme* (PASTIS) was conceived in particular to minimize *peak locking* effects. The scheme was based on a small interrogation region to be correlated with a

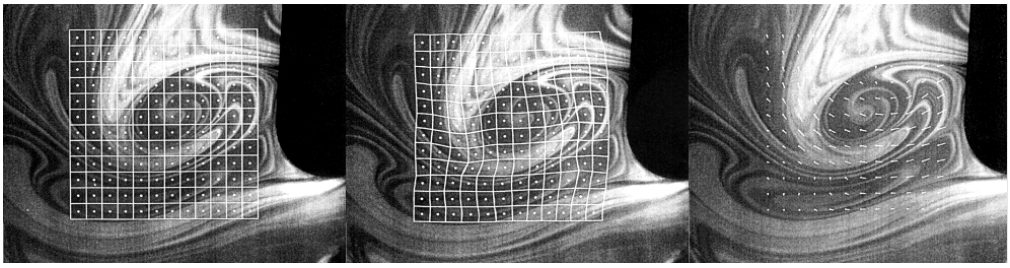

Figure 11. Cylinder-wake flow. (*a*) Initial placement of series expansion neighbourhood, each square denotes a control volume; (*b*) displacement of grid after 100 ms, estimated using the nonlinear correlation process; (*c*) displacement of centres of grid over 100 ms (Tokumaru and Dimotakis 1995).

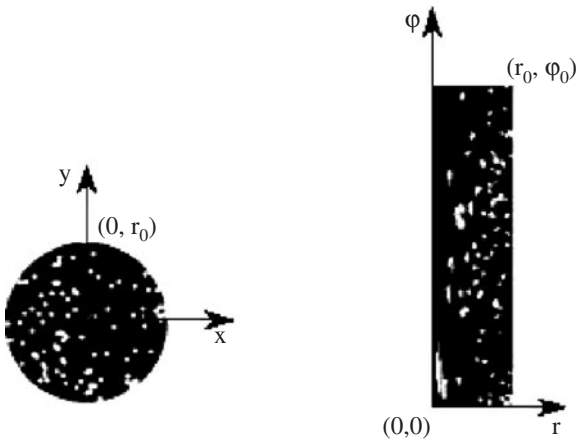

Figure 12. A PIP in x–y plane (left), and its mapped pattern MPIP in r–φ plane (Ruan *et al* 2001).

larger search area. After each iteration a progressive refinement of the spatial resolution is applied. The displacement field distribution is estimated with an earlier interrogation from which the image transformation is applied such that the search box is centred on the predicted location prior to evaluating again the residual displacement by correlation. The distorted image is reconstructed by means of a two-dimensional spline scheme.

The method shows interesting performances (assessed with synthetic images of known displacement distribution) in terms of spatial resolution, and dynamic range of velocity and vorticity.

The authors report that most of the RMS error in the basic algorithm is due to the deformation of the *continuum*. The uncertainty level is drastically reduced when the image distortion is applied, as shown in figure 13. Conversely, it seems evident that most of the *peak locking* error linked to the pixelization of the images is compensated when the latter are treated with a fractional offset procedure.

A performance assessment with synthetic images of a DNS flow field was also proposed, showing the global impact of the method on the measurement in turbulent flows. Clearly, the measurement precision benefits from the introduction of the continuous domain transformation, as shown in figure 14.

Quenot *et al* (1998) proposed an approach based on orthogonal dynamic programming (ODP). Optical flow computation consists of evaluating the displacement distribution from a sequence of images on the assumption that the image intensity is conserved during the motion. The technique introduced by Quenot (1992) as the orthogonal dynamic programming (ODP-PIV) algorithm represents an extension of the technique for the detection of sub-pixel displacements from a pair of single-exposure PIV recordings. The DP algorithm that performs image strip matching was derived from a speech recognition algorithm where segments of a speech signal are transformed into a two-dimensional (time–frequency) strip representation.

Instead of the square interrogation boxes used in conventional cross-correlation analysis, the ODP method performs the matching by strip-to-strip comparison between the two images. The images are sliced into parallel and overlapping strips (figure 15). Corresponding strips are aligned and the matching is performed minimizing the relative Minkowsky distance (in the present case L_1) between the strips. A global image matching constraint is applied that enhances the methods robustness. Performing several passes with orthogonal slicing directions solves the problem of matching two-dimensional image strips.

Several advantages are reported in such an approach with respect to the cross-correlation method: (a) the interrogation returns a dense displacement field (it is possible to obtain the displacement at each single pixel); (b) the method is suitable to analyse sequences of more than two images; (c) the global image matching is performed that enforces data continuity yielding a more robust measurement; (d) local correlation is iterated over regions at high velocity, improving the measurement accuracy.

The results of the analysis on synthetic PIV images report of error level of 0.5 pixels for an image pair and of 0.2 pixels for four images.

Lin and Perlin (1998) applied the concept of sub-pattern (smaller than the interrogation window) analysis to the interrogation of PIV recordings with a large velocity gradient. Although iterative methods showed that significant improvements can be achieved in terms of spatial resolution and accuracy, nevertheless most of them relied on a proper displacement field estimate to be obtained by means of conventional cross-correlation.

When the velocity gradient is larger than allowed for in the first interrogation (e.g. when dealing with a boundary layer flow), then a proper velocity and velocity gradient estimate will not be available in that region and the first-step interrogation will not provide for a suitable predictor. As a consequence, the whole iterative method will not progress towards the measurement over the specified region.

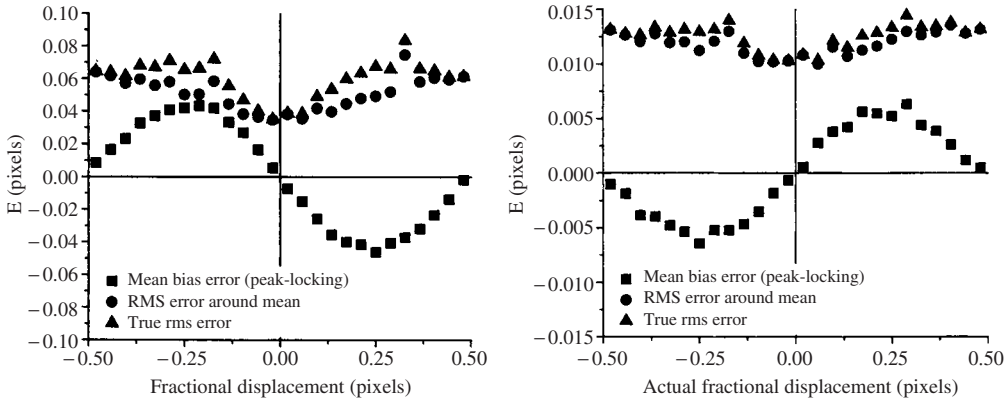

Figure 13. Error as a function of the actual fractional displacement for CIV algorithms. (Left) Basic CIV; (right) CIV with PASTIS and deformation. Remark: vertical axes have different scales (Fincham and Delerce 2000).

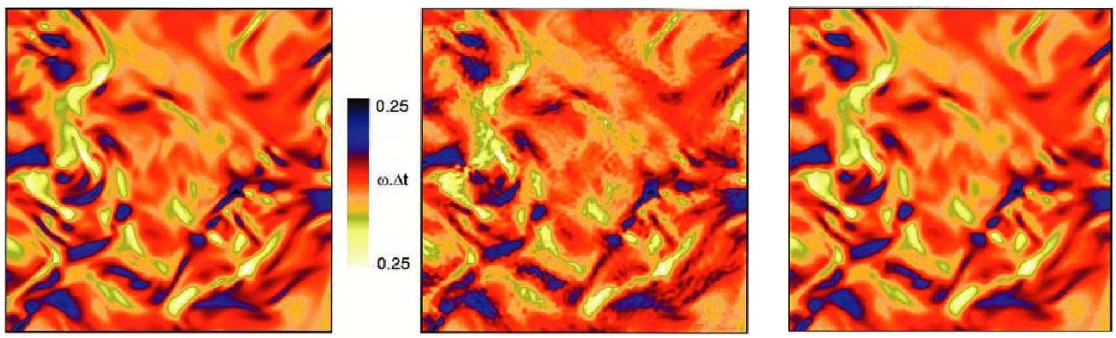

Figure 14. Vorticity field from DNS particle simulation. Left: actual vorticity; centre: standard CIV analysis (1024^2 pixels image, 15^2 pixels windows); right: CIV analysis with PASTIS and deformation (Fincham and Delerce 2000).

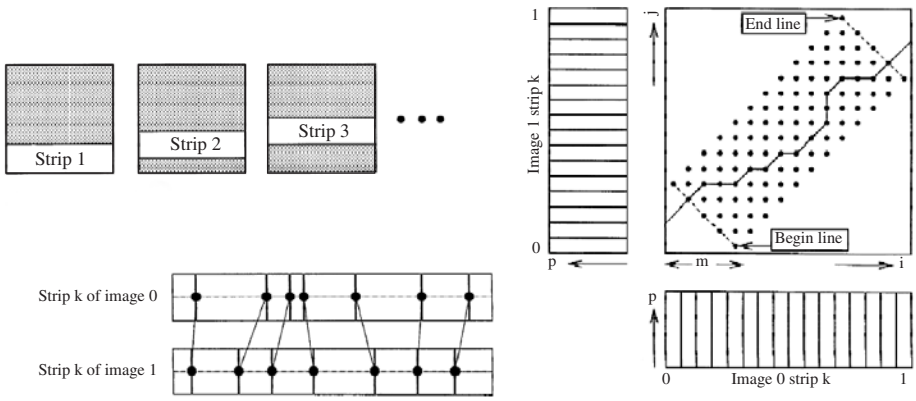

Figure 15. Dynamic programming. Image strips (top left); strip alignment (bottom left); image strips and the matching path (right).

As discussed by Keane and Adrian (1990) and Keane *et al* (1995) some criteria have to be fulfilled to optimize the interrogation of a velocity field by correlation analysis. In particular, a minimum number of particle images (at least 12) must be present in the interrogation window (image density). At the same time, the maximum velocity gradient has a maximum value given by

$$\left|\frac{\partial u}{\partial x}\right|\Delta t < \frac{d}{D} \tag{3.8}$$

where Δt is the time separation between the two exposures, D is the window size and d is the mean particle image diameter.

Finally, the one-quarter rule is suggested to limit the loss of pairs due to in-plane motion.

Often one or more of the above criteria cannot be satisfied in certain flow regions because the minimum window size (with respect to the minimum number of particle images) is too large with respect to the constraint on the velocity gradient. Thus, the iterative process fails at its start and never converges. The sub-pattern interrogation method proposed by Lin and Perlin makes use of sub-interrogation windows smaller than the original interrogation window, circumventing the difficulty in fulfilling the optimality criteria.

The method combines the information obtained from the analysis at sub-pattern level to extract a suitable prediction of the velocity gradient within the entire correlation window (figure 16). The prediction is therefore given as the linear image distortion. The performance assessment made with synthetic images shows that the restriction on large velocity gradient is significantly relaxed as compared with conventional cross-correlation.

4. Sub-pixel interpolation

4.1. Particle image sub-pixel interpolation

PIV interrogation methods that employ a continuous image displacement distribution require an image re-sampling process that yields the image intensity at intermediate locations between the pixel array.

It has to be remarked that the image re-sampling process is a crucial step for the appropriate reconstruction of the image signal (Pratt 1978). A variety of interpolation or regression methods that may be applied from the simplest linear interpolation to more refined schemes. A suitable image interpolation method should avoid loss of information in the re-sampling process.

In the present discussion several schemes have been introduced. However, one should bear in mind that the PIV image signal spectrum has a major component on the high-frequency side. Therefore, the adopted scheme requires a spectral response that respects the constraints coming from sampling theory, i.e. the Nyquist criterion.

Two-dimensional linear interpolation is therefore inappropriate and higher-order polynomial forms are preferred, although they require a larger computational cost.

The cardinal function interpolation formula (Hall 1979) fulfils the above prerequisite:

$$R(x, y) = \sum_{i=-\infty}^{i=+\infty} \sum_{j=-\infty}^{j=-\infty} f(i, j) \times \frac{\sin[\pi (i - x)]}{\pi (i - x)} \frac{\sin[\pi (j - y)]}{\pi (j - y)}. \tag{4.1}$$

Here, $R(x, y)$ represents the image intensity retrieved at a sub-pixel location ($[x, y] \in \Re^2$) from the discrete image array $f(i, j)$. From the image sampling theory this interpolation allows reconstruction of the image without loss of information if the original signal (image) has been sampled according to the Nyquist criterion.

Clearly, the reconstruction scheme cannot be applied following the above equation since the *sinc* function continues to both positive and negative infinity. Therefore, only a limited number of neighbouring pixels are considered, resulting in a truncated-sinc filter kernel and the summation is computed over $M + 1$ points in each direction. The computational effort for the image interpolation increases with the square of M and it can be fairly intensive when $M > 6$. However, the truncated-sinc filter response shows excessive ripple in the pass-band (Gibbs effect) resulting from the abrupt discontinuity at the ends of the truncated sinc function.

A simple method of improving the response consists in the multiplication of the truncated-sinc by a Hamming or a Blackman window (Niblack 1986). The idea is to reduce the abruptness of the truncated ends. When the truncated-sinc is windowed by a smooth function, a smooth frequency response is returned:

$$\begin{gathered} w(i) = 0.54 - 0.46 \cos(2\pi i/M) \\ \text{(1D Hamming window)} \\ w(i) = 0.42 - 0.5 \cos(2\pi i/M) + 0.08 \cos(4\pi i/M) \\ \text{(1D Blackman window).} \end{gathered} \tag{4.2}$$

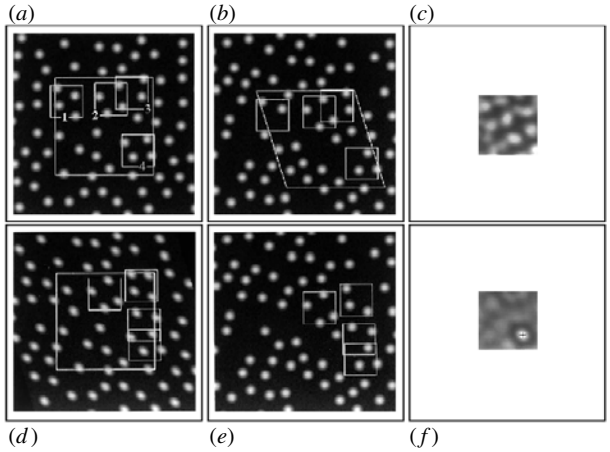

Figure 16. Step-by-step results of the sub-pattern PIV procedure. (*a*) Interrogation window (large square) and sub-pattern windows; (*b*) candidate set of displacement vectors (small squares) and related interrogation window deformation; (*c*) sub-pattern '2' cross-correlation map; (*d*) full-size distorted interrogation window; (*e*) different choice of sub-pattern windows for further iterations; (*f*) cross-correlation signal after window distortion.

4.2. Correlation peak sub-pixel interpolation

Since the precision of the measurement is directly linked to that of the peak location in the correlation map, it is clear that the structure of the correlation map as a whole and in particular that of the peak were the subject of well-focused studies. Since the introduction of peak fitting functions for sub-pixel displacement estimates (Willert and Gharib 1991), a number of anomalies were progressively found from analytical and numerical studies concerned with the accuracy of the fractional displacement estimators.

The three most frequently reported peak interpolation or fitting schemes are the centroid, parabolic and Gaussian (based on a three-by-three pixels kernel). The accuracy of the fractional displacement estimate associated with the above schemes has been widely studied and detailed results from theoretical and numerical investigations were given by Westerweel (1993), Lourenço (1996), Raffel *et al* (1998), Nogueira *et al* (1999) among others.

More sophisticated schemes that involve two-dimensional interpolation or convolution reconstruction were also widely investigated (Ronnerberger *et al* 1998, Lourenço 1999, Sugii *et al* 2000). In some cases it appeared that the existing forms of systematic error of the fractional displacement initially ascribed to an improper peak fit method were to be found in the structure of the discrete correlation map itself (Westerweel 1997, Fincham and Delerce 2000).

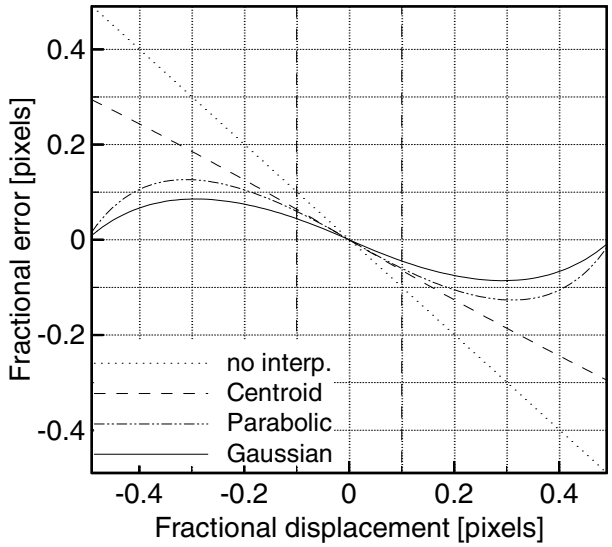

Figure 17. Tracking error $\hat{\varepsilon}$–ε for common peak-fit functions and for the closest integer estimate (no interpolation). Vertical lines indicate the typical RMS uncertainty of cross-correlation analysis.

Commonly it was found that for cross-correlation analysis a main bias term underestimates the displacement with a periodic behaviour of one pixel wavelength. It was clear that the source of this kind of error must be sought for in the image pixelization and in the consequent discrete nature of the correlation signal.

Several arguments help clarify the periodic error of one pixel wavelength that occurs when we try to recover sub-pixel information from the correlation table. As discussed by Westerweel (1993), for a typical choice of the peak fit function (three-point Gaussian) the fractional error pattern resembles that outlined in figure 17 where the centroid and the parabolic scheme are also plotted for comparison.

In this example, the Gaussian scheme shows the best performance. This result is confirmed by several authors and implicitly supported by the broad application of the Gaussian scheme in the research community.

Independently of the interpolating function, the error vanishes when the fractional displacement approaches zero. If no interpolation scheme is used, the error equals the fractional displacement, thus it is maximized at ± 0.5 pixels. In this case the displacement values are *locked* at integer values because the returned domain is given by the integer numbers.

Adopting an interpolation scheme still shows a bias of the displacement estimate towards integer values. In particular, the effects are visible when field quantities such as vorticity or rate of strain are displayed which amplify the measurement noise. Although the *peak locking* effect occurs with a regular pattern, it is not possible to remove it *a posteriori*, subtracting it from the measured value. In fact, the unknown phase of the error is embedded into the random noise.

The above problem can be properly treated with methods that try to compensate for this form of error.

If the exact particle displacement is known, then a local shift can be applied between the correlating areas before evaluating the correlation. Therefore a zero fractional displacement is obtained and the associated bias error vanishes. However, since the actual particle image displacement is not known *a priori*, only a prediction can be assumed to be available from a previous interrogation. Thus, the behaviour of the displacement estimate should be investigated when a relative offset is applied between the two correlating windows with the precision of a displacement predictor. Assessment of cross-correlation performances widely reported in the literature (Huang *et al* 1997, Raffel *et al* 1998) over a wide range of simulation parameters shows that in typical conditions (32×32 pixel window, five pixel displacement, ten particle/window, moderate gradient) the RMS error ε_r does not exceed one-tenth of a pixel.

The improvement in accuracy can be estimated by comparing the error due to the periodic bias (*peak locking*) effect with discrete window offset and that associated with a sub-pixel window offset method.

The fractional displacement can be modelled as a variable with uniform distribution between +0.5 and -0.5, thus the RMS tracking error ε'_b is defined as follows:

$$\varepsilon'_b \equiv \int_{-1/2}^{+1/2} (\hat{\varepsilon} - \varepsilon)^2 \, \mathrm{d}\varepsilon. \tag{4.3}$$

For the Gaussian peak-fit $\varepsilon'_b = 0.062$. After the application of the sub-pixel window offset it can be assumed that the residual displacement is a statistical variable with zero mean and uniform distribution with an amplitude given by ε'_b. Consequently, the expression of the residual *peak locking* bias in the case of sub-pixel window offset becomes

$$\varepsilon'_b* \equiv \frac{1}{2\varepsilon_r} \int_{-\varepsilon'_b}^{+\varepsilon'_b} (\hat{\varepsilon} - \varepsilon)^2 \, \mathrm{d}\varepsilon. \tag{4.4}$$

Thus, depending on the RMS uncertainty, this form of error can be reduced significantly, while its upper limit is given by the *peak locking* error given by the discrete window offset. For the Gaussian peak fit, $\varepsilon'_b* = 0.011$.

According to this model procedure the bias error on the displacement estimate becomes negligible in comparison with the random error.

Algorithms that use such a technique imply that the image has to be reconstructed in order to retrieve the grey-level intensity at fractional locations.

Among the works that proposed the fractional window offset is that of Lecordier (1997), which also reorients the interrogation windows to minimize the velocity difference due to the velocity gradient. Results were shown from simulated PIV images reporting RMS uncertainties of the order of 10^{-2} pixel. However, the computational load of the method is significantly increased due to two factors: (1) the interrogation was performed multiple times since several iterations are performed for the result to converge; (2) the image reconstruction by interpolation is computationally intensive.

5. Spatial resolution

The spatial resolution of the interrogation method is clearly related to the minimum size of the correlation window (Keane *et al* 1995) that can be used in the image interrogation. Decreasing the size of the interrogation spot is known to be a common procedure to improve the spatial resolution.

However, it is well known that by decreasing the number of particle images per interrogation window (image density), the amount of information is also reduced and the result is more susceptible to both random correlation peaks (lower S/N, Keane and Adrian 1990, Prasad *et al* 1992) and random errors in the sub-pixel peak interpolation.

Larger interrogation windows are more robust and when the velocity gradient is sufficiently small they can provide very accurate sub-pixel displacements. However, when the length scale of the velocity fluctuations is smaller than the interrogation window the interrogation performs poorly.

Since the size of the interrogation window is limited by the particle average spacing, a high seeding density is desirable to attain a lower spatial wavelength cut-off.

The spatial response of the cross-correlation is similar to that of a spatial low-pass filter with top-hat distribution. For such a linear filter it is possible to define a modulation transfer function (Willert and Gharib 1991). The latter assumption was verified using synthetic PIV images with sinusoidal displacement distribution (Scarano and Riethmuller 2000a) as it is shown in figure 21.

Clearly, a faithful reconstruction of the velocity spatial fluctuations can be obtained when the window size does not exceed 20% of the spatial wavelength of the velocity distribution. Conversely, it is remarkable that a window size of only half the spatial wavelength returns a signal that is reduced to 60% of the original peak.

In several cases it is often unclear whether it is more important to resolve the small flow scales at the cost of an increased measurement noise or to obtain a low-pass flow representation with a higher smoothness. In the first case the data set is not directly suitable for differentiation and low-pass filtering will be needed anyway.

Further suggestions to improve the spatial resolution have been proposed in the literature, namely hybrid methods that combine the robust pattern matching capability of cross-correlation together with the large data/particle yield, which is typical of individual particle tracking techniques. Such an approach proposed by Keane *et al* (1995) under the name of super-resolution PIV has led to several developments (Cowen and Monismith 1996, van der Plas and Bastiaans 1998, Ishikawa *et al* 2000, Takehara *et al* 2000, Wernet 2001 and others). However, the PTV technique and related methods will not be discussed in the present context.

Among the super-resolution methods, sub-pattern interrogation can also be mentioned (Lin and Perlin 1998, Nogueira *et al* 2001, Lourenço and Krothapalli 1998).

6. An iterative image deformation interrogation algorithm

The remainder of this paper describes in detail the practical implementation of the WIDIM iterative image distortion interrogation algorithm (Scarano and Riethmuller 1998).

The technique is based on the PID methodology proposed by Huang *et al* (1993) and is implemented as a hierarchical scheme that allows a progressive refinement of the window size. As a result, the method progressively compensates for the in-plane flow motion at smaller scale iteration after iteration.

The application of hierarchical schemes for the multi-resolution analysis of PIV images is currently widespread and although different approaches are proposed for its implementation, there is a general agreement about its effectiveness (Kumar and Banerjee 1998, Fincham and Delerce 2000, Nogueira *et al* 2000).

A brief description of the basic principle of the method is as follows:

(1) The PIV images are interrogated with a basic cross-correlation method with a relatively coarse grid. The window size is chosen so as to fulfil the basic interrogation criteria such as the one-quarter rule. Results are validated so as to not include spurious data in further steps.
(2) The result of the correlation is used to build a predictor displacement field over all the image pixels. A bilinear interpolation is used for this purpose.
(3) The two images are deformed according to the predictor spatial distribution. Since both the images compensate for half of the displacement, the measurement is centred on the original pixel location, resulting in a second-order accurate estimate of the displacement. The image deformation involves the re-sampling of the pixel values at intermediate locations, therefore an interpolation is applied (cardinal function interpolation formula).
(4) The interrogation window size is reduced according to a pre-defined refinement step.
(5) The images are interrogated, yielding a displacement field with a finer resolution.
(6) The velocity result is validated with respect to prescribed criteria.
(7) The validated velocity distribution is then used as a final output or as an iterative input to point (2). The interrogation process is repeated until a convergence criterion is satisfied.

6.1. Performance assessment

To assess in detail the performance of the algorithm a systematic analysis was carried out by means of a reference particle image displacement field applied to synthetic particle images. Particles' light imaging and tracers' motion were simulated to build benchmark PIV images. Different types of displacement distribution were investigated: uniform translation, uniform shear and sinusoidal displacement. A detailed description of the simulation is given in Scarano and Riethmuller (2000).

Particle images with a Gaussian profile were artificially generated at locations randomly distributed in space. The pixel intensity level ($I \in [0, 1 \ldots 255]$) was obtained by integration of the Gaussian distribution over a virtual array sensor (pixel fill factor 1.0). Particle peak intensity and diameter were also modelled as random variables ($I_p = 80, \sigma_{Ip} = 80$; $d_p = 2$ pixels, $\sigma_{dp} = 1$). A particle density of 0.10 particle/pixel was obtained generating 6554 particles over an array of 256×256 pixels.

The spatial wavelength response of the technique was tested over a reference sinusoidal displacement distribution. Different sizes of the interrogation window were tested. The sinusoidal displacement distribution is uniform along the x-coordinate of amplitude $A = 2$ pixels and wavelength Λ

varying in the range from 8 to 128 pixels. The reference response was assumed to be that of a single low-pass filter (moving average) with a rectangular window of the same size as the interrogation spot.

6.2. Results

Figure 20 shows the mean displacement error pattern associated with different correlation-based interrogation procedures when a uniform displacement is applied. The systematic underestimation for the conventional correlation (labelled with triangles) agrees with Westerweel (1993) and Raffel *et al* (1998). The discrete window offset method (labelled with squares) compensates for this effect, but it suffers from a periodic bias associated with the fractional displacement. Moreover, the offset at the closest integer introduces a discontinuity when the fractional displacement equals 0.5 pixels. The bias error associated with the sub-pixel window offset procedure (labelled with diamonds) is significantly smaller since it keeps below 5×10^{-3} pixels.

The behaviour of the RMS error is one of the most important outcomes of the simulation (figure 1, right).

The data series related to the basic cross-correlation lies at about 0.1 pixels, while the multigrid iterative discrete offset technique yields a result about half an order of magnitude below. Considering a displacement of ten pixels as the reference maximum displacement, the discrete offset technique yields a dynamic range of 2.5 orders of magnitude. When the fractional window displacement is applied, the error is drastically reduced at about 10^{-3} pixels resulting in a dynamic range of almost four orders of magnitude.

7. Towards adaptive resolution

The method discussed in the previous section shows the potential of hierarchical schemes yielding multigrid flow image analysis. However, the progressive window refinement is applied uniformly over the entire image and it is therefore independent of the local flow features.

When dealing with highly inhomogeneous flows (shear flows, compressible flows) a high spatial resolution might be required only in some parts of the investigated domain, whereas large parts of the flow might require information with lower spatial density.

In terms of signal analysis, it is desirable that the spatial response of the interrogation method be adapted with respect to the spatial scale of the signal to be analysed (namely, velocity distribution).

Recalling the diagram in figure 18, it is desirable to apply a window size that is proportional to the wavelength of the spatial velocity fluctuations.

The method proposed herein aims at suppressing the unnecessary constraint that the interrogation window size should be constant over the whole domain of analysis. Similarly to what is obtained in the field of computational fluid dynamics (CFD), with solution adaptive domain discretization with unstructured meshing, the measurement or evaluation points should be chosen with a density according to the wavelength of the local spatial velocity fluctuations.

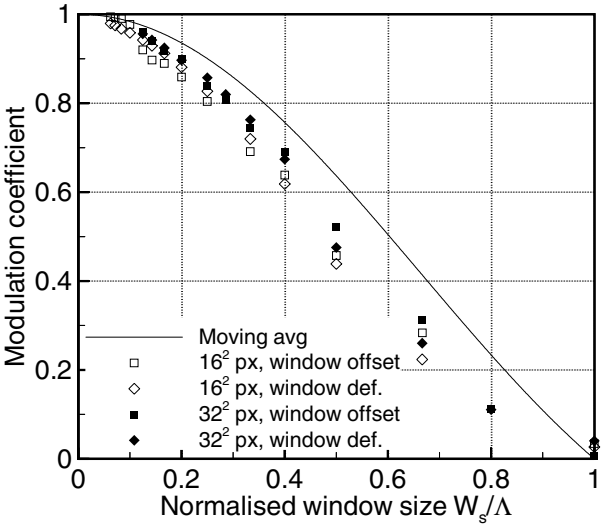

Figure 18. Spatial response of the correlation analysis to a sinusoidal displacement distribution.

The local radius of curvature $r(x, y)$ of the scalar velocity distribution gives a suitable description of the spatial wavelength of the velocity fluctuation $\Lambda(x, y)$. The velocity components are regarded as functions of two independent variables: the spatial coordinates. Therefore, the minimum local curvature radius is given by the inverse of the maximum eigenvalue of the Hessian matrix $H_u(x, y)$ defined as

$$H_u(x, y) = \begin{bmatrix} u_{xx} & u_{xy} \\ u_{yx} & u_{yy} \end{bmatrix}. \tag{7.1}$$

For a non-singular matrix the eigenvalues problem yields

$$\begin{gathered} \lambda^2 - \lambda(u_{xx} + u_{yy}) - u_{xy}^2 = 0 \\ \lambda_{1,2} = \frac{u_{xx} + u_{yy}}{2} \pm \sqrt{\left(\frac{u_{xx} + u_{yy}}{2}\right)^2 - u_{xy}^2}. \end{gathered} \tag{7.2}$$

Finally the local curvature radius is expressed by

$$r(x, y) = \frac{1}{\max\{\lambda_1, \lambda_2\}}. \tag{7.3}$$

For a sinusoidal displacement distribution the relation between the spatial wavelength and the curvature radius is

$$\Lambda = 2\pi\sqrt{r}. \tag{7.4}$$

According to a linear response of the spatial cross-correlation operator (Scarano and Riethmuller 2000) the effect of spatial modulation depends on the ratio between the window linear size W_s and spatial wavelength Λ of the velocity fluctuation.

A linear relation can be applied between Λ and the local spatial sampling length expressed in terms of the mean distance h between neighbouring interrogation points:

$$h = a + b\Lambda. \tag{7.5}$$

The window linear size W_s and the sampling length are related through the window overlap factor $OF = 1 - h/W_s$. Once the window overlap (typically 50 or 75%) has been chosen it is

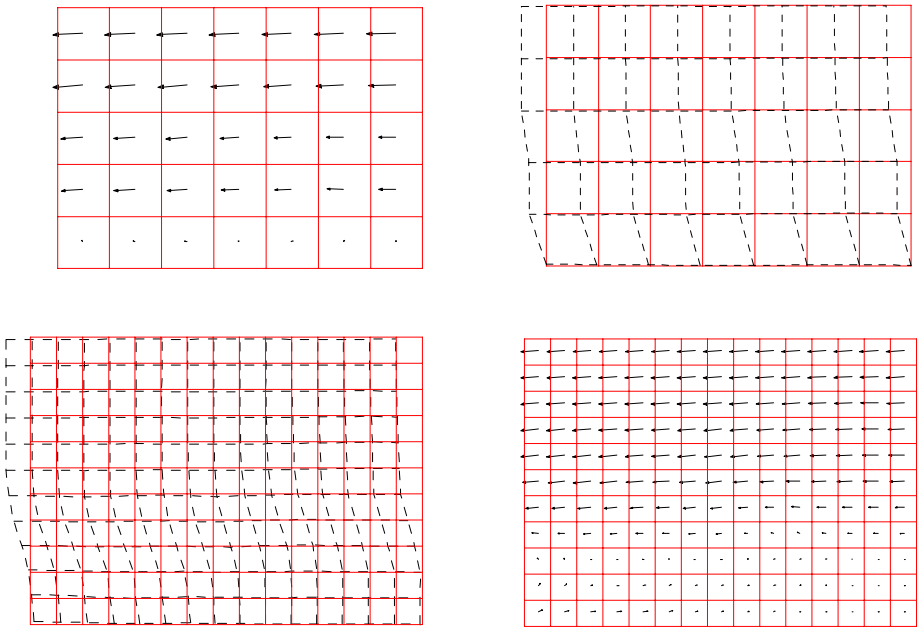

Figure 19. Multigrid image deformation method. Top left: interrogation grid and result of cross-correlation on the coarse grid; top right: image deformation at the resolution of the coarse grid; bottom left: image deformation at the resolution of the refined grid; bottom right: interrogation grid and result of cross-correlation on the refined grid.

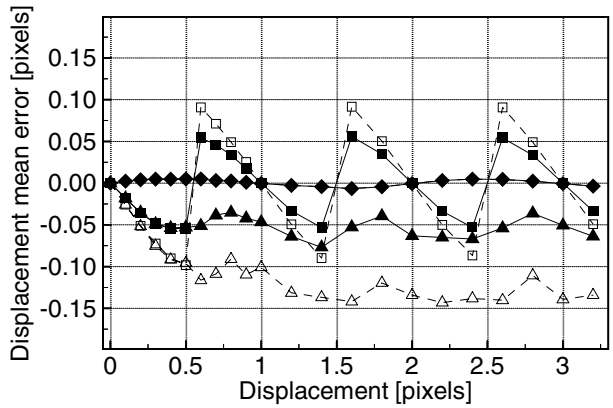

Figure 20. Mean displacement error as a function of the displacement for different window sizes and interrogation procedures. Full symbols 32×32 pixels and empty symbols 16×16 pixels analysis: ▲ basic cross-correlation; ■ discrete window offset; ♦ iterative multigrid window deformation. Corresponding RMS error is given in figure 1, right (Scarano and Riethmuller 2000).

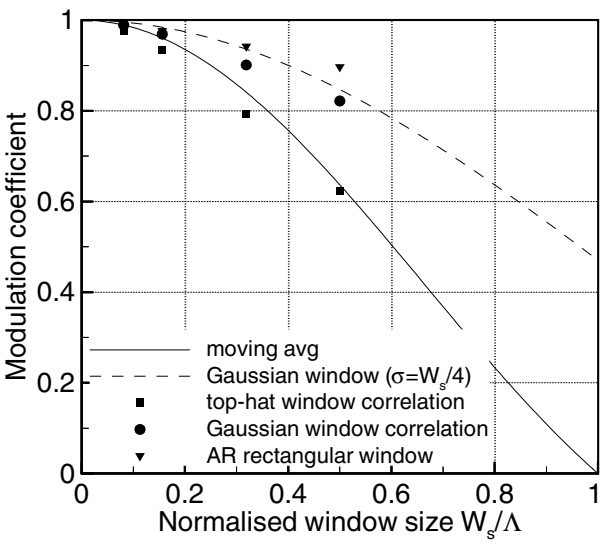

Figure 21. Spatial response of the AR correlation analysis for a sinusoidal displacement distribution.

possible to establish a direct relation between the local velocity fluctuation wavelength and the interrogation window size:

$$W_s = \frac{a + b\Lambda}{1 - OF}. \tag{7.6}$$

The constant a is determined by the minimum size of the interrogation window size. This parameter is related to the size and the spatial density (in pixels) of the particle images. Typically $a \in [8, 32]$ pixels. Conversely, the constant b expresses the direct relation between the spatial wavelength of the velocity fluctuations and the spatial response of the interrogation element. The choice $b < 1$ yields a modulation effect below 5%.

The whole technique relies on the knowledge of the actual velocity spatial distribution, which is not known *a priori* and which is the objective of the measurement procedure itself. Therefore, the above concepts of adaptive spatial sampling density and interrogation window size are implemented in the image analysis technique within a recursive structure. The result of each single interrogation is used as an input to evaluate the interrogation parameters for the subsequent iteration. The process terminates either when a convergence criterion is fulfilled or after a prescribed number of iterations. Typically after five iterations the results reached convergence, and further iterations do not add any significant accuracy improvement.

When the method is applied to a sinusoidal displacement

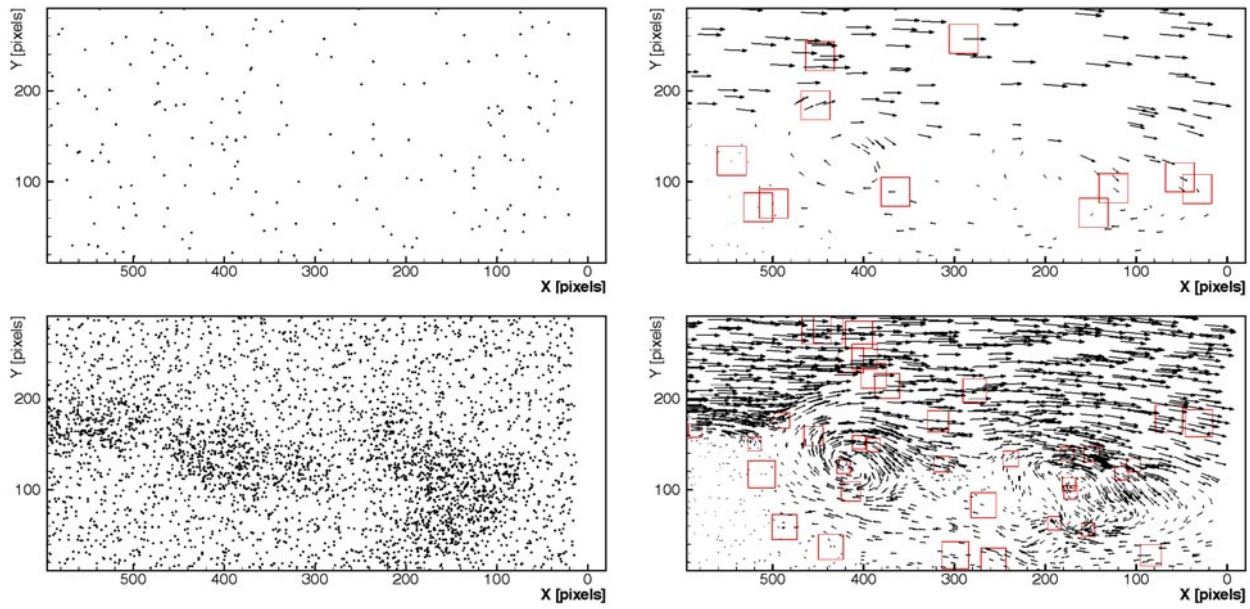

Figure 22. Image analysis with the iterative adaptive resolution scheme: random interrogation locations chosen at the beginning of the process (top left); velocity vector distribution from cross-correlation (top right); refined and adapted interrogation points distribution at the third iteration (bottom left); velocity vector distribution from cross-correlation (bottom right). Dense areas correspond to smaller interrogation windows.

field, the response of the adaptive resolution method can be evaluated in terms of spatial modulation. Figure 21 shows the results from the sinusoidal displacement simulation. The modulation transfer function of rectangular and Gaussian linear filter ($\sigma = W_s/4$) is also plotted for reference.

The data series relative to the local refinement method shows that it is possible to minimize the modulation effect; nevertheless, such a process must take into account the lower limit for the window size.

7.1. Experimental assessment

Completeness requires that the proposed method performance be evaluated over real experimental conditions in order to verify the outcomes of the simulated PIV images.

The turbulent flow over a backward-facing step flow is considered to be a valuable a test case since it contains several features of interest, such as the sharp separation with a steep velocity profile in the free mixing layer and a large spectrum of scales developing downstream. Several investigations are still devoted to this subject due to the complex flow behaviour (Le *et al* 1997, Huang and Fiedler 1997, Scarano and Riethmuller 1999, 2000, among others).

The experiments are performed in a gravity-driven water tunnel of $240(w) \times 120(h)$ mm^2 cross section. The contraction ratio between the settling chamber and the test section is 6:1. The channel step is placed 760 mm downstream of the contraction.

The step expansion ratio is in the present case $ER = 1.2$. The light source is a double cavity pulsed Nd:Yag laser. Two semi-cylindrical lenses and a spherical lens are used to shape the laser beam into a 0.8 mm thick light sheet. Latex particles (25 μm diameter) are used to seed the flow.

The image acquisition system is composed of a CCD video sensor PCO-SensiCam with 1280 $\times$ 1024 pixel resolution, 12 bits quantization. Measurements are performed in the plane of symmetry over a region extending from the $x/h = -1$ up to 8.

Experiments are conducted at $Re_h = 5.0 \times 10^3$, and the free stream velocity $U_0 = 0.125$ m s^{-1} (evaluated at $x/h = -1$). The typical time separation between the two laser pulses of 5 ms is selected so as to obtain a maximum in-plane displacement of about 0.5 mm (five pixels).

The image processing is performed with three image distortion iterations. The interrogation window size ranges from 15 $\times$ 15 pixels to 31 $\times$ 31 pixels and an overlap factor of 75% is applied between adjacent windows. The invalid data yield ($S/N < 1.5$) is 2%. An example is shown in figure 22.

The same images are analysed with the WIDIM scheme with a window size of 23×23 pixels and 75% window overlap, with an invalid data yield of 3%.

The data are obtained over an unstructured grid and are restored over a uniform Cartesian mesh by means of a two-dimensional quadratic least-squares regression. From the representation of the velocity vector distribution over a regular grid it is possible to compare the results obtained with the AR method and those coming from the interrogation on a regular mesh with uniform window size.

Figure 23 shows the improvement obtained with the adaptive resolution in terms of velocity gradient range. From the vorticity distribution it can be appreciated that the two methods have a similar performance except for the highly sheared and vortical regions where AR returns peak values about 20% higher. Finally, a direct comparison of the velocity vector distribution is also shown in figure 24. The velocity vertical profiles are shown one-in-eight for clarity. It is possible to identify those regions of the flow where the AR methods brings a significant improvement: in the left side of the picture the intense shear layer emanating from the step edge attains values of the strain rate as high as 0.5 pixel/pixel. Further

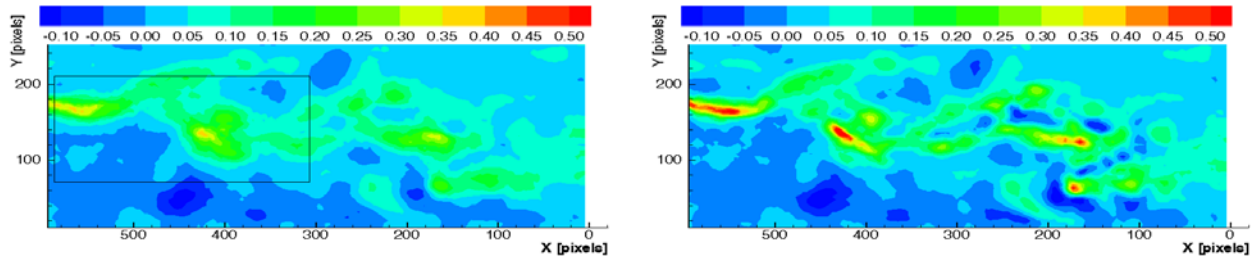

Figure 23. Instantaneous vorticity distribution (pixels/pixel). Uniform window size 23 × 23 pixels (left); adaptive window size 31 × 31 → 15 × 15 pixels (right).

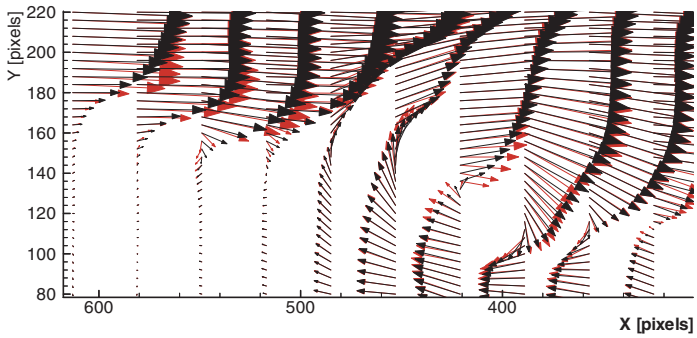

Figure 24. Instantaneous velocity distribution (flow detail from figure 23). Uniform window size (black) and AR (red). A one-in-eight velocity vertical profile is shown for clarity.

downstream a vortex roll-up exhibits a similar value of the vorticity.

It is worth remarking that the data constitute the raw output of the image evaluation and no spatial filtering or post-processing is applied to the velocity vector data except for the necessary interpolation from the unstructured to the Cartesian mesh. A two-dimensional quadratic least-squares regression is applied to evaluate the velocity at the structured grid locations.

8. Conclusions

The overview of PIV interrogation techniques has shown that the cross-correlation method constitutes the basis of a wide variety of algorithms in particle image motion analysis. The discussion began with the statement that the digital PIV image recording technique opened the development of interrogation algorithms of higher performances with respect to optical methods. The general features of the digital correlation algorithm were recalled and the main drawbacks were discussed, such as the limit of the velocity and vorticity dynamic range due to in-plane *loss of pairs*. The typical problems occurring during the cross-correlation analysis were explained, showing the cross-correlation of a pair of single-exposure digital PIV recordings.

The problem of the limited velocity range was handled successfully with the introduction of a second-step interrogation with the offset of the interrogation area or, equivalently, performing the correlation search over a larger extent with respect to the interrogation area. The resulting method allows minimization of the dependence between the velocity dynamic range and the spatial resolution.

Concerning the discrete window offset technique (described as the simplest two-step adaptive scheme) the CDI method that shifts both windows equally with respect to the centre of the interrogation location yields a better accuracy without additional computational cost.

Among the most difficult forms of error to correct for is the bias due to *peak locking*, which is inherent to the digital imaging hardware. This problem seems to be addressed by the introduction of schemes that apply the window offset with a sub-pixel precision. Techniques that apply the sub-pixel window offset method (PID, WIDIM, PASTIS) showed improvements in accuracy of about one order of magnitude.

Direct computation of the image flow velocity and its derivatives (CIV, DMV) was demonstrated to be a viable approach, although the performances on the determination of the velocity gradient (vorticity) have not been fully assessed.

The typical answer to the analysis of flows with a high deformation rate was given by iterative schemes. The displacement spatial distribution obtained with cross-correlation analysis is used to predict the actual particle motion and to perform the image pattern deformation. The interrogation accuracy and robustness in the presence of highly sheared flows is significantly improved with respect to the basic scheme. However, in general such advanced algorithms increase the computational cost because of their iterative structure, and most of all because of the additional image re-sampling process.

Spatial resolution was discussed in terms of spatial response of the correlation method to sinusoidal displacement distribution. It was proven that both the basic and iterative cross-correlation methods have a response that is similar to that of a top-hat filter having the same dimensions as the interrogation window. It was concluded that the major limitation on improving the spatial resolution consists in the seeding particle spatial density and the resolution of the recording devices.

A possible step towards adaptive resolution was proposed with a flow-adaptive local window refinement scheme that shrinks the interrogation window according to the local curvature of the velocity components. As a result, the spatial response of the AR method returned a significant improvement showing a lower modulation effect.

The performance assessment of the AR-WIDIM method was completed with an experimental verification made with PIV images of a turbulent flow over a BFS. In the comparative analysis the method showed an improved robustness and accuracy, especially with respect to the highly sheared flow region. As an overall impression, the window deformation method returned a lower noise level and small-scale fluctuations were measured with a higher precision.

In conclusion, several efforts were reported in the development of methods based on iterative cross-correlation and image deformation over the last decade. It is the author's opinion that the PIV technique has already reached its maturity concerning the image processing methods, therefore further studies in this direction might not repeat the improvements obtained so far. However, it is expected that marginal developments could bring further improvements with respect to the interrogation robustness (data validation) and the spatial resolution with AR or hybrid methods.

References

Adrian R J 1988 Statistical properties of particle image velocimetry measurements in turbulent flow *Laser Anemometry in Fluid Mechanics—III* (Lisbon: Instituto Superior Tecnico) pp 115–19

Adrian R J 1991 Particle-imaging techniques for experimental fluid mechanics *Ann. Rev. Fluid Mech.* **23** 261–304

Boillot A and Prasad A K 1996 Optimization procedure for pulse separation in cross-correlation PIV *Exp. Fluids* **21** 87

Cho Y-C 1989 Digital image velocimetry *Appl. Opt.* **28** 740–8

Cowen E A and Monismith S G 1996 A hybrid digital particle tracking velocimetry technique *Exp. Fluids* **22** 199–201

Fincham A M and Delerce G 2000 Advanced optimization of correlation imaging velocimetry algorithms *Exp. Fluids* **29** S013–22

Fincham A M and Spedding G R 1997 Low cost, high resolution DPIV for measurement of turbulent fluid flow *Exp. Fluids* **23** 449–62

Guezennec Y G and Kiritsis N 1990 Statistical investigation of errors in particle image velocimetry *Exp. Fluids* **10** 138–46

Gui L, Longo J and Stern F 2001 Biases of PIV measurement of turbulent flow and the masked correlation-based interrogation algorithm *Exp. Fluids* **30** 27–35

Gui L and Merzkirch W 2000 A comparative study of the MQD method and several correlation-based PIV evaluation algorithms *Exp. Fluids* **28** 36–44

Gui L, Merzkirch W and Fei R 2000 A digital mask technique for reducing the bias error of the correlation-based PIV interrogation algorithm *Exp. Fluids* **29** 30–5

Hall E L 1979 *Computer Image Processing and Recognition* (New York: Academic)

Hart D P 1998 The elimination of correlation errors in PIV processing *9th Int. Symp. on Applications of Laser Techniques to Fluid Mechanics (Lisbon, Portugal, July 1998)*

Hart D P 2000 DPIV error correction *Exp. Fluids* **29** 13–22

Hesselink L 1988 Digital image processing in flow visualization *Ann. Rev. Fluid Mech.* **20** 421–85

Horn B K P and Schunck B G 1981 Determining optical flow *Artif. Intell.* **17** 185–203

Huang H, Dabiri D and Gharib M 1997 On errors of digital particle image velocimetry *Meas. Sci. Technol.* **8** 1427–40

Huang H T and Fiedler H E 1997 A DPIV study of a starting flow downstream of a backward-facing step *Exp. Fluids* **23** 395–404

Huang H T, Fielder H F and Wang J J 1993a Limitation and improvement of PIV, part I. Limitation of conventional techniques due to deformation of particle image patterns *Exp. Fluids* **15** 168–74

Huang H T, Fielder H F and Wang J J 1993b Limitation and improvement of PIV, part II. Particle image distortion, a novel technique *Exp. Fluids* **15** 263–73

Ishikawa M, Murai Y, Wada A, Iguchi M, Okamoto K and Yamamoto F 2000 A novel algorithm for particle tracking velocimetry using the velocity gradient tensor *Exp. Fluids* **29** 519–31

Jambunathan K, Ju X Y, Dobbins B N and Ashforth-Frost S 1995 An improved cross correlation technique for particle image velocimetry *Meas. Sci. Technol.* **6** 507–14

Keane R D and Adrian R J 1990 Optimization of particle image velocimeters. Part 1: double pulsed system *Meas. Sci. Technol.* **1** 1202–15

Keane R D and Adrian R J 1992 Theory of cross correlation analysis of PIV images *J. Appl. Sci. Res.* **49** 191–215

Keane R D, Adrian R J and Zhang Y 1995 Super-resolution particle imaging velocimetry *Meas. Sci. Technol.* **6** 754–68

Kimura I and Takamori T 1986 Image processing of flow around a circular cylinder by using correlation technique *Flow Visualization IV* ed C Veret pp 2334–6

Kumar S and Banerjee S 1998 Development and application of a hierarchical system for digital particle image velocimetry to free-surface turbulence *Phys. Fluids* **10** 160–77

Le H, Moin P and Kim J 1997 Direct numerical simulation of turbulent flow over a backward facing step *J. Fluid Mech.* **330** 349–74

Lecordier B 1997 Etude de l'interaction de la propagation d'une flamme premelangée avec le champ aerodynamique, par association de la tomographie Laser et de la Vélocimétrie par Images de particules *Thèse de doctorat* de l'Université de Rouen

Lin J H and Perlin M 1998 Improved methods for thin, surface boundary layer investigations *Exp. Fluids* **25** 431–44

Lourenço L 1996 Particle image velocimetry *Particle Image Velocimetry (Von Kármán Institute Lecture Series 1996-03)* (Belgium: Rhode-Saint Genése)

Lourenço L 1999 Particle image and tracking velocimetry *Optical Diagnostics of Particles and Droplets (Von Kármán Institute Lecture Series 1999-01)* (Belgium: Rhode-Saint Genése)

Lourenço L and Krothapalli A 1995 On the accuracy of velocity and vorticity measurements with PIV *Exp. Fluids* **18** 421–8

Lourenço L and Krothapalli A 1998 Mesh-free second order accurate algorithm for PIV processing *Proc. Int. Conf. on Optical Technology and Image Processing in Fluid, Thermal and Combustion Flows (Yokohama, Japan, Dec. 1998)* p 224

Niblack W 1986 *An Introduction to Digital Image Processing* (Englewood Cliffs, NJ: Prentice-Hall)

Nogueira J, Lecuona A and Rodriguez P A 1999 Local field correction PIV: on the increase of accuracy of digital PIV systems *Exp. Fluids* **27** 107–16

Nogueira J, Lecuona A and Rodriguez P A 2001 Identification of a new source of peak locking, analysis and its removal in conventional and super-resolution PIV techniques *Exp. Fluids* **30** 309–16

Plas van der G A J and Bastiaans R J M 1998 Accuracy and resolution of a fast PTV-algorithm suitable for HIRES-PIV *Proc. 8th Int. Symp. Flow Vis. (Sorrento, Italy)*

Prasad A K, Adrian R J, Landreth C C and Offutt P W 1992 Effect of resolution on the speed and accuracy of particle image velocimetry interrogation *Exp. Fluids* **13** 105–16

Pratt W K 1978 *Digital Image Processing* (New York: Wiley)

Quenot G M 1992 The orthogonal algorithm for optical flow detection using dynamic programming *Proc. IEEE ICASSP* **3** 249–52

Quenot G M, Pakleza J and Kowalewsky T A 1998 Particle image velocimetry with optical flow *Exp. Fluids* **25** 177–89

Raffel M, Willert C E and Kompenhans J 1998 *Particle Image Velocimetry, a Practical Guide* (Berlin: Springer)
Riethmuller M L (ed) 2000 *Particle Image Velocimetry and Associated Techniques, VKI LS 2000-01* (Rhode-Saint Genese, BE: Von Karman Institute)
Rohaly J, Nakajiama T and Ikeda Y 2000 Identification of true particle image displacement based on false correlation symmetry at poor signal peak detectability *Exp. Fluids* **29** S023–33
Ruan X, Song X and Yamamoto F 2001 Direct measurement of the vorticity field in digital particle images *Exp. Fluids* **30** 696–704
Scarano F, Benocci C and Riethmuller M L 1999 Pattern recognition analysis of the turbulent flow past a backward facing step *Phys. Fluids* **11** 3808–18
Scarano F and Riethmuller M L 1998 Perfectionnement dans les techniques de traitement des données en vélocimétrie par images de particules *Actes 6ème Congrès Francophone de Vélocimétrie, Laser (Saint-Louis, France)*
Scarano F and Riethmuller M L 1999 Iterative multigrid approach in PIV image processing *Exp. Fluids* **26** 513–23
Scarano F and Riethmuller M L 2000a Advances in iterative multigrid PIV image processing *Exp. Fluids* **29** S051–60
Scarano F and Riethmuller M L 2000b Temporal analysis of coherent structures in a turbulent BFS flow with PIV *10th Int. Symp. on Applications of Laser Techniques to Fluid Mechanics (Lisbon, Portugal)*
Sugii Y, Nishio S, Okuno T and Okamoto K 2000 A highly accurate iterative PIV technique using a gradient method *Meas. Sci. Technol.* **11** 1666–73
Takehara K, Adrian R J, Etoh G T and Christensen K T 2000 A Kalman tracker for super-resolution PIV *Exp. Fluids* **29** S034–41
Tokumaru P T and Dimotakis P E 1995 Image correlation velocimetry *Exp. Fluids* **19** 1–15
Utami T and Ueno T 1984 Visualization and picture processing of turbulent flow *Exp. Fluids* **2** 25–32
Utami T and Ueno T 1991 A cross-correlation technique for velocity field extraction from particulate visualization *Exp. Fluids* **10** 213–23
Wernet M P 2001 New insights into particle image velocimetry data using fuzzy-logic-based correlation/particle tracking processing *Exp. Fluids* **30** 434–47
Wereley and Meinhart 2000 Accuracy improvements in particle image velocimetry algorithms. PIV *10th Int. Symp. on Applications of Laser Techniques to Fluid Mechanics, (Lisbon, Portugal)*
Westerweel J 1993 Digital particle image velocimetry *PhD Dissertation* Delft University Press, Delft
Westerweel J 1994 Effcient detection of spurious vectors in particle image velocimetry data *Exp. Fluids* **16** 236–47
Westerweel J 1997 Fundamentals of digital particle image velocimetry *Meas. Sci. Technol.* **8** 1379–92
Westerweel J 2000 Theoretical analysis of the measurement precision in particle image velocimetry *Exp. Fluids* **29** S3–12
Westerweel J, Dabiri D and Gharib M 1997 The effect of a discrete window offset on the accuracy of cross-correlation analysis of digital PIV recordings *Exp. Fluids* **23** 20–8
Willert C E and Gharib M 1991 Digital particle image velocimetry *Exp. Fluids* **10** 181–93